GEOPHYSICS, VOL. 71, NO. 1 (JANUARY-FEBRUARY 2006); P. I1–I9, 7 FIGS.
10.1190/1.2159050

Geophysical Software and Algorithms

A spectral numerical method for electromagnetic diffusion

José M. Carcione[1]

ABSTRACT

I present a pseudospectral explicit scheme that can simulate low-frequency electromagnetic (EM) propagation in the earth. This scheme solves linear periodic parabolic equations, having accuracy within machine precision, both temporally and spatially. The method is based on a Chebyshev expansion of the evolution operator, with the spatial derivatives computed via a staggered Fourier pseudospectral technique. The results match analytical solutions of the initial-value problem and the Green's function. An example of the EM field produced by a set of magnetic sources in a heterogeneous model illustrates the algorithm's performance.

INTRODUCTION

Electromagnetic (EM) modeling and propagation at low frequencies (EM diffusion) is used in a number of applications: geothermal exploration (Pellerin et al., 1996), evaluation of hydrocarbon resources by mapping subseafloor resistivity (Everett, 1990; Unsworth et al., 1993; Eidesmo et al., 2002), EM induction in boreholes and logging while drilling (Badea et al., 2001; Wang and Signorelli, 2004), magnetotelluric problems (Mackie et al., 1993; Zyserman and Santos, 2000; Yin and Maurer, 2001; Mitsuhata and Uchida, 2004), and geoelectrical surveys for groundwater and mineral exploration (Oristaglio and Hohmann, 1984).

Most existing modeling schemes are restricted to plane layers or have finite accuracy because of the low-order approximations of the time and space derivatives, since they are based mostly on finite-difference and finite-element methods. A spectral method for hyperbolic equations, based on a Chebyshev expansion, has been proposed by Tal-Ezer (1986). Applications of this method can be found in Tal-Ezer and Kosloff (1984) (Schrödinger equation), Tal-Ezer et al. (1987) (acoustic-wave equation), Carcione et al. (1988) and Tal-Ezer et al. (1990) (viscoelastic equation), Muir et al. (1992) (elastic wave equation), and De Raedt et al. (2003) (Maxwell's wave equation). Most of these authors use the standard Fourier method to compute the spatial derivatives (Kosloff and Baysal, 1982). To my knowledge, the only spectral algorithm proposed for the Maxwell diffusion equation is that of Druskin and Knizhnerman (1994). It is based on a global Krylov subspace (Lanczos) approximation of the solution in the time and frequency domains.

In this work, I develop a spectral modeling method for the propagation of low-frequency signals. The algorithm uses an explicit scheme based on a Chebyshev expansion of the evolution operator in the domain of the eigenvalues of the propagation matrix (Tal-Ezer, 1989). The spatial derivates are computed with the staggered Fourier pseudospectral method (Fornberg, 1996; Carcione, 1999). The algorithm has solved the 1D telegraph equation for electric drillstring telemetry (Carcione and Poletto, 2003). The Chebyshev method, either for parabolic or hyperbolic problems, has spectral accuracy in time and space and therefore avoids numerical dispersion, a characteristic feature of low-order schemes.

THE TRANSVERSE ELECTRIC (TE) AND TRANSVERSE MAGNETIC (TM) MAXWELL'S EQUATIONS

In 3D vector notation, Maxwell's equations, neglecting displacement currents, are

$$\nabla \times \mathbf{E} = -\mu \partial_t (\mathbf{H} + \mathbf{M}) \tag{1}$$

and

$$\nabla \times \mathbf{H} = \sigma (\mathbf{E} + \mathbf{J}) \tag{2}$$

Peer-reviewed code related to this article can be found at software.seg.org/2006/0001.
Manuscript received by the Editor February 14, 2005; revised manuscript received May 18, 2005; published online January 4, 2006; publisher error corrected January 5, 2006.
[1]Istituto Nazionale di Oceanografia e di Geofisica Sperimentale (OGS), Borgo Grotta Gigante 42c, 34010 Sgonico, Trieste, Italy. E-mail: jcarcione@ogs.trieste.it.

(Sanders and Reed, 1986), where **E** and **H** are the electric and magnetic fields, **J** is the electric source, **M** is the magnetic source, μ is the magnetic permeability, σ is the electrical conductivity, and ∂_t denotes a partial derivative with respect to the time variable. In general, these quantities depend on the Cartesian coordinates (x, y, z) and the time variable t. Equations 1 and 2 constitute six scalar equations with six scalar unknowns, since **M** and **J** are known.

Maxwell's equations can be written in terms of the electric field **E** or the magnetic field **H** as

$$\sigma\partial_t\mathbf{E} = -\nabla\times(\mu^{-1}\nabla\times\mathbf{E}) - \partial_t(\nabla\times\mathbf{M}) - \sigma\partial_t\mathbf{J} \quad (3)$$

and

$$\mu\partial_t\mathbf{H} = -\nabla\times(\sigma^{-1}\nabla\times\mathbf{H}) - \mu\partial_t\mathbf{M} + \nabla\times\mathbf{J}. \quad (4)$$

Let us assume that the material properties and the source are invariant in the y-direction. Then, the propagation can be described in the (x, z)-plane, and E_x, E_z, and H_y are decoupled from E_y, H_x, and H_z, corresponding to the so-called transverse magnetic (TM) and transverse electric (TE) equations, respectively.

Writing equation 3 in explicit Cartesian form results in

$$\sigma\partial_t\begin{pmatrix}E_x\\E_z\end{pmatrix} = \begin{pmatrix}\partial_z\mu^{-1}\partial_z & -\partial_z\mu^{-1}\partial_x\\ -\partial_x\mu^{-1}\partial_z & \partial_x\mu^{-1}\partial_x\end{pmatrix}\begin{pmatrix}E_x\\E_z\end{pmatrix} - \partial_t\begin{pmatrix}-\partial_z M_y\\ \partial_x M_y\end{pmatrix} - \sigma\partial_t\begin{pmatrix}J_x\\J_z\end{pmatrix}, \quad (5)$$

where ∂_x and ∂_z denote the spatial derivatives. Equation 4 is

$$\mu\partial_t H_y = \partial_x(\sigma^{-1}\partial_x H_y) + \partial_z(\sigma^{-1}\partial_z H_y) - \mu\partial_t M_y + (\partial_z J_x - \partial_x J_z). \quad (6)$$

The respective TE equations are

$$\sigma\partial_t E_y = \partial_x(\mu^{-1}\partial_x E_y) + \partial_z(\mu^{-1}\partial_z E_y) - \partial_t(\partial_z M_x - \partial_x M_z) - \sigma\partial_t J_y \quad (7)$$

and

$$\mu\partial_t\begin{pmatrix}H_x\\H_z\end{pmatrix} = \begin{pmatrix}\partial_z\sigma^{-1}\partial_z & -\partial_z\sigma^{-1}\partial_x\\ -\partial_x\sigma^{-1}\partial_z & \partial_x\sigma^{-1}\partial_x\end{pmatrix}\begin{pmatrix}H_x\\H_z\end{pmatrix} - \mu\partial_t\begin{pmatrix}M_x\\M_z\end{pmatrix} + \begin{pmatrix}-\partial_z J_y\\ \partial_x J_y\end{pmatrix}. \quad (8)$$

I consider equations 6 and 7 to obtain the Green's function and the solution from an initial condition (see Appendix A).

PHASE VELOCITY, ATTENUATION FACTOR, AND SKIN DEPTH

The phase velocity v_p and attenuation factor α can be obtained from the complex velocity (see equation A-4) as

$$v_p = [\mathrm{Re}(v^{-1})]^{-1} \quad \text{and} \quad \alpha = -\omega\mathrm{Im}(v^{-1}) \quad (9)$$

(Carcione, 2001), respectively, where Re and Im denote real and imaginary parts. The skin depth, the effective distance of penetration of the signal, is the distance d for which $\exp(-\alpha d) = 1/e$, where e is Napier's number. Using equation A-4 yields

$$v_p = 2\pi f d \quad \text{and} \quad \alpha = \frac{1}{d}, \quad (10)$$

and

$$d = \sqrt{\frac{a}{\pi f}}, \quad (11)$$

where $f = \omega/2\pi$ is the frequency and where

$$a = \frac{1}{\mu\sigma}. \quad (12)$$

NUMERICAL ALGORITHM

Equations 5–8 have the form

$$\frac{\partial\mathbf{w}}{\partial t} = \mathbf{G}\mathbf{w} + \mathbf{s}, \quad (13)$$

where **w** is the field vectors $(E_x, E_z)^\top$, H_y, E_y, and $(H_x, H_z)^\top$, respectively; **s** is the source vector (the last two terms in each equation); and **G** is the propagation matrix:

$$\mathbf{G} = \sigma^{-1}\begin{pmatrix}\partial_z\mu^{-1}\partial_z & -\partial_z\mu^{-1}\partial_x\\ -\partial_x\mu^{-1}\partial_z & \partial_x\mu^{-1}\partial_x\end{pmatrix}, \quad (14)$$

$$\mathbf{G} = \mu^{-1}(\partial_x\sigma^{-1}\partial_x + \partial_z\sigma^{-1}\partial_z), \quad (15)$$

$$\mathbf{G} = \sigma^{-1}(\partial_x\mu^{-1}\partial_x + \partial_z\mu^{-1}\partial_z), \quad (16)$$

and

$$\mathbf{G} = \mu^{-1}\begin{pmatrix}\partial_z\sigma^{-1}\partial_z & -\partial_z\sigma^{-1}\partial_x\\ -\partial_x\sigma^{-1}\partial_z & \partial_x\sigma^{-1}\partial_x\end{pmatrix} \quad (17)$$

for equations 5, 6, 7, and 8, respectively.

Spatial differentiation

The algorithm uses the staggered Fourier method, which consists of a spatial discretization and calculation of spatial derivatives using the fast Fourier transform (Canuto et al., 1987; Fornberg, 1996; Carcione, 2001). Staggered operators evaluate derivatives between gridpoints. For instance, if Δx is the grid (cell) size and k_x is the wavenumber component, a phase shift $\exp(\pm ik_x\Delta x/2)$ is applied when computing the x-derivative, where $i = \sqrt{-1}$. Then, $\partial_x\sigma^{-1}\partial_x$ is calculated as $D_x^-\sigma^{-1}D_x^+$, where $D_x^\pm$ is the discrete operator and $\pm$ refers to the sign of the phase shift. The spatial differentiation requires interpolation of the material properties at half-gridpoints (e.g., Carcione, 1999).

Chebyshev expansion for time evolution

Considering a discretization with N gridpoints, system 13 becomes a coupled system of $L\times N$ ordinary differential equations at the gridpoints, where L is the dimension of the matrix **G**. The solution to equation 13 subject to the initial condition $\mathbf{w}(0) = \mathbf{w}_0$ is formally given by

$$\mathbf{w}_N(t) = \exp(t\mathbf{G}_N)\mathbf{w}_N^0 + \int_0^t \exp(\tau\mathbf{G}_N)\mathbf{s}_N(t-\tau)d\tau, \quad (18)$$

where $\mathbf{w}_N^0$ is the initial-condition field vector, $\exp(t\mathbf{G}_N)$ is the evolution operator, and the subscript N indicates that those quantities are discrete representations of the respective continuous quantities. I consider a separable source term $\mathbf{s}_N = \mathbf{a}_N f(t)$, where $\mathbf{a}_N$ is the spatial distribution of the source and the function $f(t)$ is the source time history. A discrete solution of equation 18 is achieved by approximating the evolution operator. For instance, in the absence of a source, the solution can be expressed by

$$\mathbf{w}_N(t) = H_M(t\mathbf{G}_N)\mathbf{w}_N^0, \tag{19}$$

where H_M is a polynomial of degree M that converges to $\exp(t\mathbf{G}_N)$ in the domain that includes all eigenvalues of operator $t\mathbf{G}_N$. I use the following Chebyshev expansion of $\exp(x)$:

$$\exp(x) = \sum_{k=0}^{\infty} a_k(bt)T_k\left(\frac{x}{bt}\right), \tag{20}$$

(Abramowitz and Stegun, 1972, p. 71; Tal-Ezer, 1989), where a_k are the expansion coefficients, T_k is the Chebyshev polynomial of order k, and b is the absolute value of the eigenvalue of matrix $\mathbf{G}_N$ having the largest negative real part. (As we shall see later, the eigenvalues are located on the real axis and their real part is negative.) For convergence, $|x| \le bt$ and x lies on the real axis. The expansion coefficients are given by

$$a_k(u) = c_k I_k(u), \quad c_0 = 1, \quad c_k = 2, \quad k \ge 1; \tag{21}$$

I_k is the modified Bessel function of order k.

Let us perform the change of variable

$$y = \frac{1}{bt}(x + bt), \quad -1 \le y \le 1. \tag{22}$$

From equations 20 and 22,

$$\exp(x) = \exp(-bt)\exp(bty) = \sum_{k=0}^{\infty} b_k T_k(y), \tag{23}$$

where

$$b_k = a_k \exp(-bt) = c_k \exp(-bt) I_k(bt) \tag{24}$$

for initial conditions without source and

$$b_k = c_k \int_0^t \exp(-b\tau) I_k(b\tau) f(t-\tau) d\tau \tag{25}$$

in the presence of a source (without initial conditions). The reason for the change of variable x to y is to avoid calculating Bessel functions when the argument bt is large, since this may exceed the dynamic range of the computer. Instead, the quantity $\exp(-bt)I_k(bt)$ is computed.

For computations, expansion 23 must be truncated. Thus, the M degree polynomial approximation of $\exp(x)$ is

$$H_M(x) = \sum_{k=0}^{M} b_k T_k(y(x)). \tag{26}$$

Because x in equation 20 is replaced by $t\mathbf{G}_N$, the variable y defined in equation 22 is represented by an operator $\mathbf{F}_N$ defined as

$$\mathbf{F}_N = \frac{1}{b}(\mathbf{G}_N + b\mathbf{I}), \tag{27}$$

where $\mathbf{I}$ is the identity matrix of dimension L. In the absence of sources, the discrete solution is

$$\mathbf{w}_N^M(t) = \sum_{k=0}^{M} b_k(t) T_k(\mathbf{F}_N)\mathbf{w}_N^0. \tag{28}$$

The value $T_k(\mathbf{F}_N)\mathbf{w}_N^0$ is computed by using the recurrence relation of the Chebyshev polynomials,

$$T_k(u) = 2uT_{k-1}(u) - T_{k-2}(u), \qquad k \ge 2, \tag{29}$$

and

$$T_0(u) = 1, \quad T_1(u) = u \tag{30}$$

(Abramowitz and Stegun, 1972). Hence,

$$T_k(\mathbf{F}_N)\mathbf{w}_N^0 = 2\mathbf{F}_N T_{k-1}(\mathbf{F}_N)\mathbf{w}_N^0 - T_{k-2}(\mathbf{F}_N)\mathbf{w}_N^0, \quad k \ge 2 \tag{31}$$

and

$$T_0(\mathbf{F}_N)\mathbf{w}_N^0 = \mathbf{w}_N^0, \quad T_1(\mathbf{F}_N)\mathbf{w}_N^0 = \mathbf{F}_N\mathbf{w}_N^0. \tag{32}$$

The algorithm is a three-level scheme since it uses the recurrence relation. The first time step should be larger than the duration of the source. Results at small time steps to compute time histories at specified points of the grid do not require significant additional computational effort. A slight modification of equation 28 can be used:

$$\mathbf{w}_N^M(t') = \sum_{k=0}^{M} b_k(t') T_k(\mathbf{F}_N)\mathbf{w}_N^0 \tag{33}$$

for $t < t'$. This calculation does not require significantly more computations since the terms involving the spatial derivatives $T_k(\mathbf{F}_N)\mathbf{w}_N^0$ do not depend on the time variable and are calculated in any case. Only the coefficients b_k are time dependent, such that additional sets of Bessel functions need to be computed.

My presented algorithm has infinite accuracy in time and in space, and it is highly efficient, since the stability condition requires a time step $\Delta t = O(1/N)$ compared with $\Delta t = O(1/N^2)$ for finite-order explicit schemes. Moreover, the error in time decays exponentially. Tal-Ezer (1989) carries out an error and stability analysis for the equation $\partial_t U - G\partial_{xx}U = 0$, where $G = 1$ and $N = 64$. If M indicates the minimum number of applications of the operator $t\mathbf{F}_N\mathbf{w}_N$, he shows that the Chebyshev method requires $M = 96$ to be stable against $M = 768$ for a modified Euler scheme. Regarding accuracy, he obtains $M = 70$ (present method) versus $M = 20\,000$ (Euler method) for $N = 32$ and $t = 1$ and for an L_2-error equal to 10^{-6}. Tal-Ezer's (1989) last test involves a variable coefficient problem with $G = a(x)\partial_{xx} + b(x)\partial_x + c(x)$. An L_2-error less than 10^{-8} requires $M = 100$ (present method) versus $M = 480$ (Euler method) for $N = 64$ and $t = 1$. Despite the 1D character of the equations, these verifications are general regarding the dimensionality of the space, since the spatial derivates are performed by the pseudospectral Fourier method, which has been widely used and tested for hyperbolic equations (e.g., Tal-Ezer et al., 1987).

Eigenvalues of the propagation matrix

In the Fourier domain, the time derivative is replaced by $i\omega$, where ω is the angular frequency; the spatial derivatives ∂_x and ∂_z are replaced by ik_x and ik_z, where k_x and k_z are the components of the wavenumber vector. Then the eigenvalue equation in the complex λ-domain ($\lambda = i\omega$), corresponding to the eigensystems represented by the propagation matrices 14 and 17, is

$$\lambda(\lambda + ak^2) = 0, \tag{34}$$

where a is defined in equation 12 and $k^2 = k_x^2 + k_z^2$. The eigenvalues are $\lambda = 0$ and $\lambda = -ak^2$ and therefore are real and negative. On the other hand, the eigenvalue corresponding to matrices 15 and 16 is

$$\lambda = -ak^2. \tag{35}$$

The maximum wavenumber components are the Nyquist wavenumbers, which for grid spacings Δx and Δz are $k_x = \pi/\Delta x$ and $k_z = \pi/\Delta z$. They are related to the highest harmonics of the spatial Fourier transform. Hence, the value of b is

$$b = a\pi^2 \left(\frac{1}{\Delta x^2} + \frac{1}{\Delta z^2} \right). \tag{36}$$

As Tal-Ezer (1989, eq. 4.13) shows, the polynomial order should be $O(\sqrt{bt})$. I find that

$$M = \beta\sqrt{bt} \tag{37}$$

is enough to obtain stability and accuracy, where β ranges from 5 to 6. On the other hand, a safe value of M can be determined by finding the range in which the coefficients b_k differ significantly from zero (for instance, by checking the ratio b_0/b_m).

Absorbing boundaries

The boundaries of the mesh may produce wraparounds resulting from the periodic properties of the Fourier method. By analogy with the wave equation, the algorithm uses the classical damping approach for hyperbolic problems to avoid these nonphysical artifacts (Kosloff and Kosloff, 1986; Carcione, 2001). The method modifies the propagation matrix as $\mathbf{G} \rightarrow \mathbf{G} - \gamma\mathbf{I}$ in the absorbing strips around the mesh, where γ is the absorbing parameter. The complex velocity satisfies $v^2 = i\omega^2 a/(\omega - i\gamma)$ (see equation A-4), implying damping for $\gamma > 0$.

One could argue that this damping approach cannot be applied to diffusion fields because there are components of the signal traveling with almost infinite velocity. In fact, from equations 10 and 11, the phase velocity is proportional to $\sqrt{\omega}$. The fact that sources are band-limited implies that the signal travels at finite velocity; in any case, the diffusion time of the maximum of the signal is finite. Consider the Green's function A-5. The maximum in the signal at any distance r arrives at time $t = \mu\sigma r^2/4$. The signal that arrives at much earlier times is exponentially small and can be neglected. Potter (1973) refers to $\Delta t = \mu\sigma\Delta x^2/4$ as the grid diffusion time, setting the maximum time step for explicit solutions based on finite differences.

This simple damping method avoids wraparounds and reflections from the boundaries quite efficiently (see Figure 7 example). However, applying this wave-equation type of damping may not be strictly correct because the field near the absorbing strips could differ from the field of an unbounded (infinite-grid) medium. For the heat equation, it is equivalent to placing a frame of ice around the model. In this case, the frame is a metal of high conductivity. Therefore, further work is required to improve the absorbing boundary, preferably based on the use of nonperiodic boundary conditions such as Chebyshev spatial differentiation and decomposition of the diffusion field into incoming and outgoing components (e.g., Kosloff et al., 1990).

Solution approach

I solve equations 6 and 7 for H_y and E_y, respectively, and then compute $\mathbf{E}$ and $\mathbf{H}$ by using equations 1 and 2. This gives

$$\begin{pmatrix} E_x \\ E_z \end{pmatrix} = \frac{1}{\sigma} \begin{pmatrix} -\partial_z H_y \\ \partial_x H_y \end{pmatrix} \tag{38}$$

and

$$\begin{pmatrix} H_x \\ H_z \end{pmatrix} = \frac{1}{i\omega\mu} \begin{pmatrix} \partial_z E_y \\ -\partial_x E_y \end{pmatrix}. \tag{39}$$

Equations 5 and 8 have the additional eigenvalue $\lambda = 0$, which generates a static (nonpropagating) mode.

Discussion

Two basic approaches solve the diffusion equation: explicit and implicit. By performing spectral analysis of the evolution matrix $\mathbf{G}$, one can show that an explicit algorithm is related to a polynomial approximation of the function $\exp(t\mathbf{G})$ in the domain of eigenvalues of $\mathbf{G}$, while the implicit approach is related to a rational approximation of that function. Since the domain of the eigenvalues is the negative real axis, the appropriate approach is to use rational basis functions. However, using rational functions results in the need to solve linear systems. Unless one has a good preconditioner, solving linear systems is highly time consuming. This is the main reason that researchers are still exploring the explicit approach (e.g., Gallopoulos and Saad, 1992; Moret and Novati, 2001). As Gallopoulos and Saad state, "In recent years there has been a resurgence of interest in explicit methods for solving parabolic differential equations.... The main attraction of explicit methods is their simplicity.... Both the Krylov and Chebyshev algorithms (Chebyshev is used in this paper) are highly efficient explicit algorithms. The advantage of the Chebyshev method over the Krylov approach is that it does not use inner products. This feature makes the Chebyshev algorithm highly attractive in parallel computing.

SIMULATIONS

Let us consider a homogeneous medium with $\sigma = 1$ mS/m and $\mu = \mu_0 = 4\pi 10^{-7}$ H/m (magnetic permeability of a vacuum). The phase velocity and skin depth versus frequency are shown in Figure 1. The velocity increases and the skin depth decreases with frequency. Moreover, as can be inferred from

equation 11, the velocity and skin depth decrease for increasing conductivity or magnetic permeability. This means, for instance, that the diffusion process is slower in saltwater than in freshwater.

I now compare numerical and analytical solutions for the initial-value problem and the Green's function by solving equation 7 with a number of gridpoints $n_x = n_z = 120$ and grid spacing $\Delta x = \Delta z = 10$ m. The initial condition is given by equation A-14, with $\bar{k} = 0.1$/m and $\Delta k = \bar{k}/2$. Figures 2a and 3a show snapshots of the electric field (normalized) at 3 and 30 μs, respectively. The computations use $bt = 470$, $M = 130$, and $bt = 4700$, $M = 410$, respectively. The numerical (dots) and analytical solutions (solid line) along a straight line passing through the maximum of the signal are compared in Figures 2b and 3b. The amplitude ratio between the snapshots in Figures 2 and 3 is 1/0.04; the error is 0.0004% and 0.02%, respectively. (The error is computed as the L^2-norm of the difference divided by the number of gridpoints.)

Next, I consider a transient source with an initial central frequency $\bar{f} = \bar{\omega}/(2\pi) = 1$ MHz and $\Delta\omega = \bar{\omega}/2$. The comparison is shown in Figure 4 for 4 and 20 μs propagation times. The

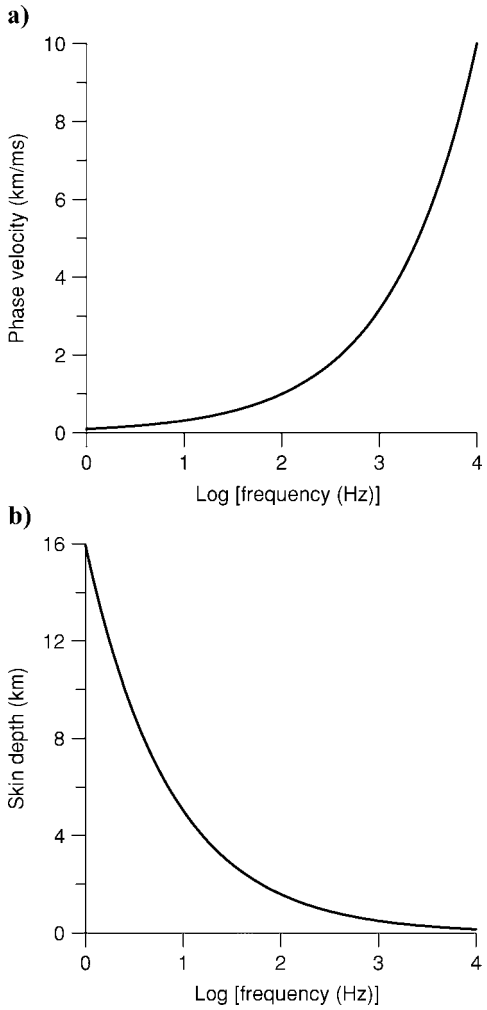

Figure 1. (a) Phase velocity and (b) skin depth versus frequency for a medium with $\mu = \mu_0$ and $\sigma = 1$ mS/m.

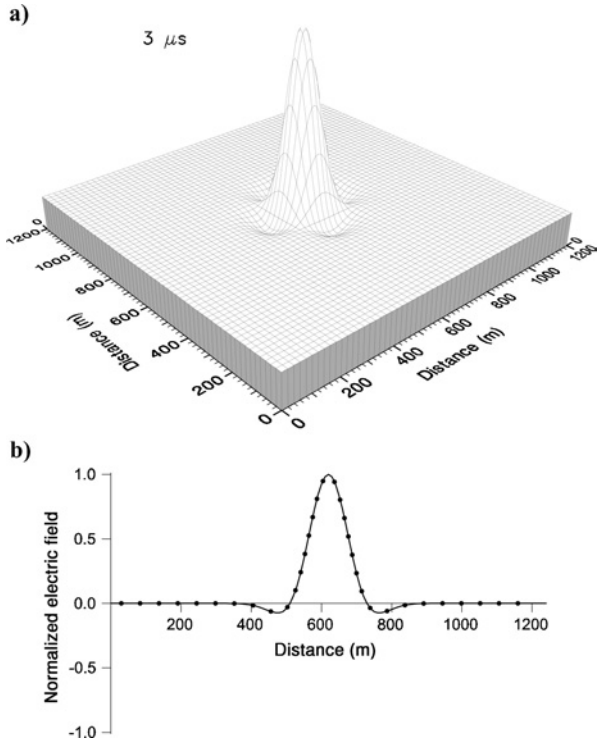

Figure 2. (a) Snapshot of the electric field (normalized) at 3 μs as a result of the initial condition A-14. (b) Comparison of the numerical and analytical solutions (dots and solid line, respectively) along a straight line passing through the maximum of the signal. The medium has $\mu = \mu_0$ and $\sigma = 1$ mS/m.

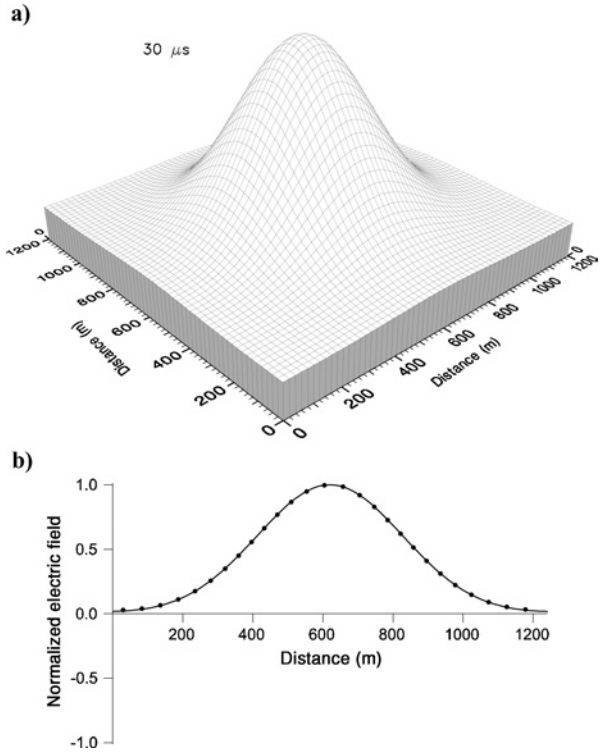

Figure 3. (a) Snapshot of the electric field (normalized) at 30 μs as a result of the initial condition A-14. (b) Comparison of the numerical and analytical solutions (dots and solid line, respectively). The medium has $\mu = \mu_0$ and $\sigma = 1$ mS/m.

first snapshot is computed by using coefficients 25; the snapshot at 30 μs is computed by starting with the solution at the first time step as the initial condition. The coefficients b_k are given by equation 24 in the latter case.

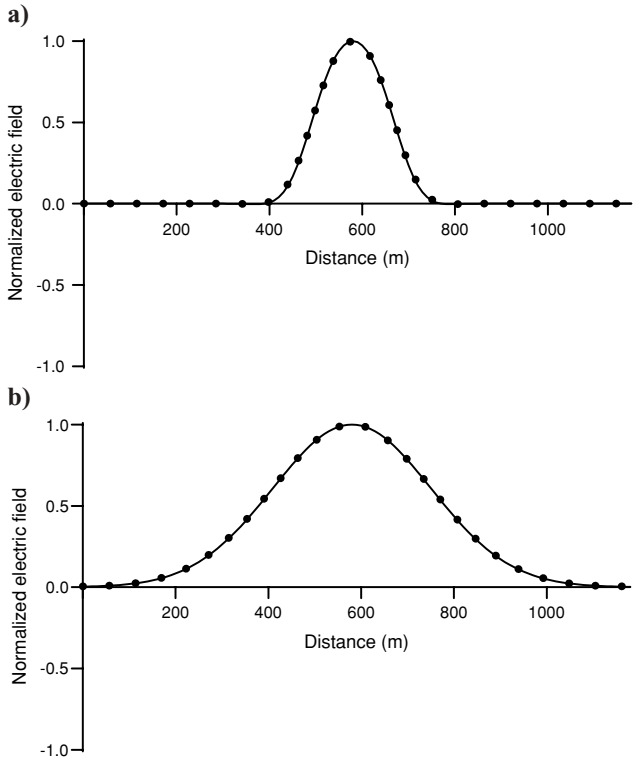

Figure 4. Snapshots of the electric field (normalized) at (a) 4 and (b) 20 μs from source A-7. The plots show the numerical and analytical solutions (dots and solid line, respectively). The medium has $\mu = \mu_0$ and $\sigma = 1$ mS/m.

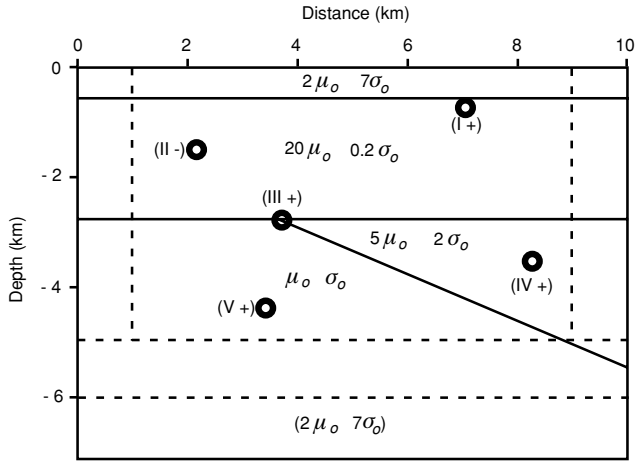

Figure 5. Inhomogeneous model with various magnetic sources denoted by Roman numerals (the sign indicates the polarity of each source). The dashed lines indicate the limits of the absorbing strips. Since the Fourier method is periodic, the strip for the upper boundary is placed at the bottom. The reference conductivity is $\sigma_0 = 1$ mS/m.

The second simulation considers the model shown in Figure 5, corresponding to an idealized inhomogeneous medium where various magnetic sources (denoted by Roman numerals) are placed (the sign indicates the polarity of each source). The dashed lines indicate the limits of the absorbing strips. Since the Fourier method is periodic, the strip for the upper boundary is placed at the bottom, with the same properties of the first row. The reference conductivity is $\sigma_0 = 1$ mS/m. I solve equation 6 with a number of gridpoints $n_x = 180$ and $n_z = 120$ and grid spacing $\Delta x = \Delta z = 60$ m. The first time step is 80 μs, corresponding to the duration of the source, which has an initial central frequency of 100 kHz. Then, 20 time steps of 120 μs are used, starting with the solution at the first time step as initial condition. The computations use $bt = 350, M = 70$, and $bt = 620, M = 150$, respectively. The number of gridpoints in the absorbing strips is 18, and the damping parameter is $\gamma = 10^5$/s.

Snapshots of the magnetic field (normalized) at 80 and 2480 μs, are shown in Figure 6. The Roman numerals refer

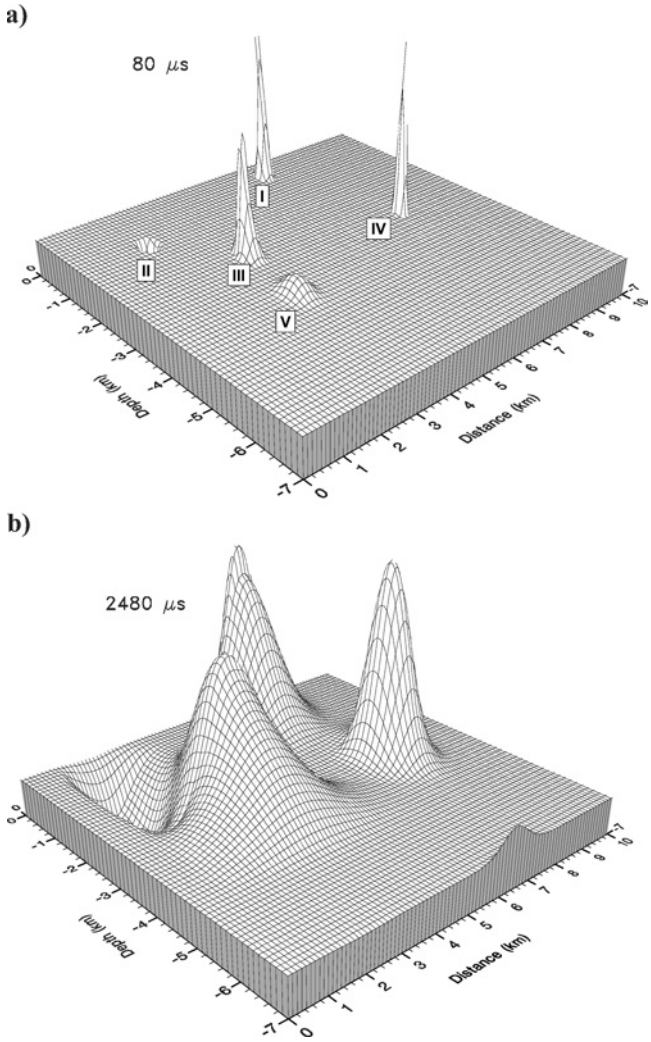

Figure 6. Snapshot of the magnetic field (normalized) at (a) 80 and (b) 2480 μs, corresponding to the model shown in Figure 5. The Roman numerals correspond to the magnetic sources. The maximum amplitude ratio (a)/(b) is 50/1.

to the magnetic sources. The field resulting from source V has a wider extension than those of the other sources. This is on account of the lower phase velocity of the field. For instance, at 50 kHz the velocities at locations IV and V are 7 and 22 km/ms, respectively. The loss of the higher frequencies is evident in Figure 6b, since the media filter the higher wavenumbers, as can be deduced from the analytical solution A-13. The performance of the absorbing strips can be recognized in the snapshots at 2480 μs. The fields caused by sources I and II reenter the mesh on the other side but are completely damped beyond a few gridpoints.

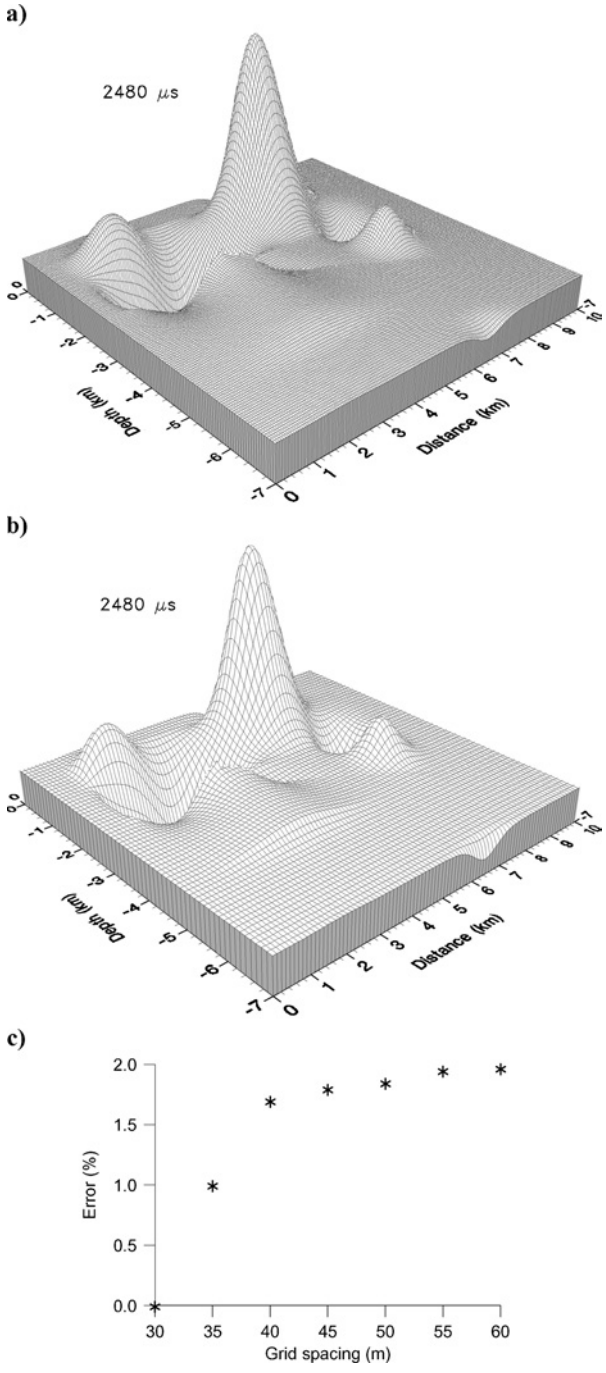

Figure 7. Snapshots of the electric-field component E_z (normalized) at 2480 μs for (a) a grid spacing $\Delta x = \Delta z = 30$ m and grid size 360 × 240 and (b) a grid spacing $\Delta x = \Delta z = 60$ m and grid size 180 × 120. (c) Error as a function of the grid spacing for seven simulations of the same model (Figure 5).

Finally, seven simulations are performed for the model shown in Figure 5, varying the grid spacing from $\Delta x = \Delta z = 30$ m to $\Delta x = \Delta z = 60$ m in 5-m steps. The grid sizes vary from 360 × 240 to 180 × 120, respectively. The wavefield between gridpoints is obtained by interpolation using the Fourier basis. Figure 7 shows snapshots of the electric-field component E_z for grid spacings of $\Delta x = \Delta z = 30$, and $\Delta x = \Delta z = 60$ m. Figure 7c shows the error as a function of the grid spacing. The error is computed as the L^2-norm of the difference between the reference snapshot (Figure 7a) and the snapshot with grid spacing $Dx(= Dz)$, divided by the L^2-norm of the reference snapshot. The CPU time ratio between the simulations shown in Figures 7a and 7b is nearly 10 (on the basis of one CPU).

CONCLUSIONS

I have developed a numerical method for modeling EM diffusion in the earth, which allows general material variability and provides snapshots and time histories of the electric and magnetic fields. Modeling at low frequencies requires an algorithm for parabolic differential equations. The algorithm is based on a Chebyshev expansion of the evolution operator. The use of this spectral method overcomes two drawbacks: low accuracy and stringent stability conditions, since the error in time decays exponentially.

Better alternatives to Chebyshev methods are basis functions of the form $a_i/(\mathbf{A} + b_i\mathbf{I})$, which are more adequate than polynomials to approximate $\exp(\mathbf{A})$, where the domain of eigenvalues is wide and on the negative real axis. To my knowledge, nobody has published an algorithm that utilizes this approach of solving linear systems, which can be very complicated and time consuming. The rational approach is very attractive only when one has a good preconditioner for the linear system. This is the main reason that effort is put on explicit algorithms like the one presented. The main advantage of the Chebyshev approach is that it does not need inner products. This is highly beneficial, especially in parallel computing. This type of problem — the number of matrix-vector multiplications needed to reach a time level using standard explicit algorithms (e.g., Runge-Kutta) — is proportional to N^{-2}, where N is the number of gridpoints. Using the Chebyshev algorithm, the number of matrix-vector multiplications is proportional only to N^{-1}. This is why my algorithm is valuable and should be used in cases where solving linear systems is highly time consuming.

Further research involves extension to three spatial dimensions, which should be straightforward with generalization to the anisotropic case and incorporation of air/ground effects. In principle, air can be modeled as a very-low-conductivity medium.

The presented algorithm can also be used to solve the diffusion equation related to other physical phenomena, such as fluid flow for reservoir simulation, slow (Biot)-wave energy diffusion, NMR resonance in porous media, and heat conduction.

ACKNOWLEDGMENTS

The author thanks Hillel Tal-Ezer, anonymous reviewers, and associate editor Joseph A. Dellinger for useful comments. This work was supported by AGIP SpA, the general director of promotions and cooperative cultures of the Italian Ministry of Foreign Affairs, and the secretary of science, technology, and product innovation of the Argentina Ministry of Education, Science and Technology.

APPENDIX A

ANALYTICAL SOLUTIONS

The modeling can be initiated either by a source or by an initial condition. Following are the respective analytical solutions.

Green's function

The Green's function corresponding to equation 7 and a source current

$$J_y(x,z,t) = I\delta(x)\delta(z)[1-H(t)] \tag{A-1}$$

is the solution of

$$\partial_t E_y = a\Delta E_y + I\delta(x)\delta(z)\delta(t), \tag{A-2}$$

where δ denotes the Dirac function, $H(t)$ is the Heaviside function, Δ is the Laplacian, and a is given by equation 12. I assume there are no magnetic sources and a homogeneous medium. Equation A-1 corresponds to shutting off a steady current I at $t=0$.

A Fourier transform to the frequency domain implies the substitution $\partial_t \to i\omega$. The diffusion equation can then be written as a Helmoltz equation:

$$\Delta E_y + \left(\frac{\omega^2}{v^2}\right) E_y = -(I/a)\delta(x)\delta(z), \tag{A-3}$$

where

$$v = \sqrt{\frac{a\omega}{2}}(1+i) \tag{A-4}$$

is the complex velocity.

Equation A-2 has the following solution (Green's function):

$$E_y(r,t) = \left(\frac{I}{4\pi a t}\right)\exp\left[\frac{-r^2}{4at}\right], \tag{A-5}$$

where

$$r = \sqrt{x^2+z^2} \tag{A-6}$$

(Carslaw and Jaeger, 1984; Polyanin, 2003).

The time-domain solution for a source $f(t)$ is obtained with a numerical time convolution between expression A-5 and $f(t)$. I use

$$f(t) = \exp\left[-\frac{\Delta\omega^2(t-t_0)^2}{4}\right]\cos[\bar{\omega}(t-t_0)], \tag{A-7}$$

where t_0 is a delay time, $\bar{\omega}$ is the central frequency, and $2\Delta\omega$ is the characteristic width of the spectrum. In this case, the coefficients b_k defined in equation 25 must be computed numerically; the spatial distribution is $\mathbf{a}(\mathbf{x}) = \delta(\mathbf{x}-\mathbf{x}_0)$, where $\mathbf{x}_0$ is the source location. For $f(t) = \delta(t)$, equation 24 is obtained.

Solution to initial condition

Equation 7 corresponding to the initial-value problem is

$$\partial_t E_y = a\Delta E_y. \tag{A-8}$$

First, I assume the initial condition $E_0 = E_y(x,z,0) = \delta(x)\delta(z)$. A triple transform of equation A-8 to the Laplace and wavenumber domains yields

$$E_y(k_x,k_z,p) = \frac{1}{p+a\left(k_x^2+k_z^2\right)}, \tag{A-9}$$

where I use the property $\partial_t E_y \to pE_y - E_0(k_x,k_z)$, $E_0(k_x,k_z)=1$.

To obtain $E_y(k_x,k_z,t)$, I compute the inverse Laplace transform of equation A-9,

$$E_y(k_x,k_y,t) = \frac{1}{2\pi i}\int_{c-i\infty}^{c+i\infty}\frac{\exp(pt)dp}{p+a\left(k_x^2+k_z^2\right)}, \tag{A-10}$$

where $c>0$. There is one pole:

$$p_0 = -a\left(k_x^2+k_z^2\right). \tag{A-11}$$

Use of the residue theorem gives the solution

$$E_y(k_x,k_z,t) = \exp\left[-a(k_x^2+k_z^2)t\right]H(t). \tag{A-12}$$

The solution for a general initial condition $E_0(k_x,k_z,0)$ is given by

$$E_y(k_x,k_z,t) = E_0(k_x,k_z,0)\exp[-a(k_x^2+k_z^2)t]H(t), \tag{A-13}$$

where I use equation A-12. (In the space domain the solution is the spatial convolution between expression A-12 and the initial condition.) The effect of the exponential on the right-hand side of equation A-13 is to filter the higher wavenumbers. The solution in the space domain is obtained by a discrete inverse Fourier transform using the fast Fourier transform.

Here, I consider the initial condition,

$$E_0(x,z,0) = \exp\left\{-\frac{\Delta k^2}{4}[(x-x_0)^2+(z-z_0)^2]\right\} \times \cos[\bar{k}(x-x_0)]\cos[\bar{k}(z-z_0)], \tag{A-14}$$

which has a Gaussian shape in the wavenumber domain,

$$E_0(k_x,k_z,0) = \frac{\pi}{\Delta k^2}F(k_x)F(k_z)\exp[-i(k_x x_0 + k_z z_0)], \tag{A-15}$$

where

$$F(k) = \exp\left[-\left(\frac{k+\bar{k}}{\Delta k}\right)^2\right] + \exp\left[-\left(\frac{k-\bar{k}}{\Delta k}\right)^2\right], \tag{A-16}$$

(x_0,z_0) is the location of the peak, $\bar{k}$ is the central wavenumber, and $2\Delta k$ is the width of the spectrum, such that $F(\bar{k}\pm\Delta k) = F(\bar{k})/e$.

REFERENCES

Abramowitz M., and I. A. Stegun, 1972, Handbook of mathematical functions: Dover Publ., Inc.

Badea E. A., M. E. Everett, G. A. Newman, and O. Biro, 2001, Finite-element analysis of controlled-source electromagnetic induction using coulomb-gauged potentials: Geophysics, **66**, 786–799.

Canuto C., M. Y. Hussaini, A. Quarteroni, and T. A. Zang, 1987, Spectral methods in fluid dynamics: Springer-Verlag New York, Inc.

Carcione J. M., 1999, Staggered mesh for the anisotropic and viscoelastic wave equation: Geophysics, **64**, 1863–1866.

———, 2001, Wave fields in real media: Wave propagation in anisotropic, anelastic and porous media, *in* K. Helbig, and S. Treitel, eds., Handbook of Geophysical Exploration, vol. 31: Pergamon Press Inc.

Carcione J. M., and F. Poletto, 2003, Electric drill-string telemetry: Journal of Computational Physics, **186**, 596–609.

Carcione J. M., D. Kosloff, and R. Kosloff, 1988, Wave propagation simulation in a linear viscoelastic medium: Geophysical Journal of the Royal Astronomical Society, **95**, 597–611.

Carslaw H. S., and J. C. Jaeger, 1984, Conduction of heat in solids: Clarendon Press.

De Raedt H., K. Michielsen, J. S. Kole, and M. T. Figge, 2003, Solving the Maxwell equations by the Chebyshev method: A one-step finite-difference time-domain algorithm: IEEE Transactions on Antennas and Propagation, **51**, 3155–3160.

Druskin V., and L. Knizhnerman, 1994, Spectral approach to solving three-dimensional Maxwell's diffusion equations in the time and frequency domains: Radio Science, **29**, 937–954.

Eidesmo T., S. Ellingsrud, L. M. MacGregor, S. Constable, M. C. Sinha, S. Johansen, F. N. Kong, and H. Westerdahl, 2002, Sea bed logging (SBL), a new method for remote and direct identification of hydrocarbon filled layers in deepwater areas: First Break, **20**, 144–151.

Everett M. E., 1990, Mid-ocean ridge electromagnetics: Ph.D. dissertation, University of Toronto.

Fornberg B., 1996, A practical guide to pseudospectral methods: Cambridge University Press.

Gallopoulos E., and Y. Saad, 1992, Efficient solution of parabolic equations by Krylov approximation methods: SIAM Journal of Scientific and Statistical Computations, **13**, 1236–1264.

Kosloff D., and E. Baysal, 1982, Forward modeling by the Fourier method: Geophysics, **47**, 1402–1412.

Kosloff D., and R. Kosloff, 1986, Absorbing boundaries for wave propagation problems: Journal of Computational Physics, **63**, 363–376.

Kosloff D., D. Kessler, A. Queiroz Filho, E. Tessmer, A. Behle, and R. Strahilevitz, 1990, Solution of the equation of dynamic elasticity by a Chebychev spectral method: Geophysics, **55**, 734–748.

Mackie R. L., T. R. Madden, and P. E. Wannamaker, 1993, Three-dimensional magnetotelluric modeling using finite difference equations — Theory and comparisons to integral equation solutions: Geophysics, **58**, 215–226.

Mitsuhata Y., and T. Uchida, 2004, 3D magnetotelluric modeling using the T-Ω finite-element method: Geophysics, **69**, 108–109.

Moret I., and P. Novati, 2001, An interpolatory approximation of the matrix exponential based on Faber polynomials: Journal of Computational Applied Mathematics, **131**, 361–380.

Muir F., J. Dellinger, J. Etgen, and D. Nichols, 1992, Modeling elastic fields across irregular boundaries: Geophysics, **57**, 1189–1193.

Oristaglio M. L., and G. W. Hohmann, 1984, Diffusion of electromagnetic fields into a two-dimensional earth: A finite-difference approach: Geophysics, **49**, 870–894.

Pellerin L., J. M. Johnston, and G. W. Hohmann, 1996, A numerical evaluation of electromagnetic methods in geothermal exploration: Geophysics, **61**, 121–130.

Polyanin A. D., 2002, Handbook of linear partial differential equations for engineers and scientists: Chapman and Hall/CRC.

Potter D., 1973, Computational physics: John Wiley & Sons.

Sanders K. F., and G. A. L. Reed, 1986, Transmission and propagation of electromagnetic waves: Cambridge University Press.

Tal-Ezer H., 1986, Spectral methods in time for hyperbolic problems: SIAM Journal of Numerical Analysis, **23**, 11–26.

———, 1989, Spectral methods in time for parabolic problems: SIAM Journal of Numerical Analysis, **26**, 1–11.

Tal-Ezer H., and R. Kosloff, 1984, An accurate and efficient scheme for propagating the time dependent Schrödinger equation: Journal of Chemical Physics, **81**, 3967–3971.

Tal-Ezer H., J. M. Carcione, and D. Kosloff, 1990, An accurate and efficient scheme for wave propagation in linear viscoelastic media: Geophysics, **55**, 1366–1379.

Tal-Ezer H., D. Kosloff, and Z. Koren, 1987, An accurate scheme for seismic forward modeling: Geophysical Prospecting, **35**, 479–490.

Temperton C., 1988, Implementation of a prime factor FFT algorithm on CRAY-1: Parallel Computing, **6**, 99–108 (cited in program accompanying this article by J. Carcione).

Unsworth M. J., B. J. Travis, and A. D. Chave, 1993, Electromagnetic induction by a finite electric dipole source over a 2-D earth: Geophysics, **58**, 198–214.

Wang T., and J. Signorelli, 2004, Finite-difference modeling of electromagnetic tool response for logging while drilling: Geophysics, **69**, 152–160.

Yin C., and H.-M. Maurer, 2001, Electromagnetic induction in a layered earth with arbitrary anisotropy: Geophysics, **66**, 1405–1416.

Zhang S., and J. Jin, 1996, Computation of special functions: John Wiley & Sons, Inc. (cited in program accompanying this article by J. Carcione).

Zyserman F. I., and J. E. Santos, 2000, Parallel finite-element algorithm with domain decomposition for three-dimensional magnetotelluric modeling: Journal of Applied Geophysics, **44**, 337–351.